HVTT16: Heavy vehicle dynamic road wear from a rigid heavy vehicle when including road crossfall

Heavy Vehicle Dynamic Road Wear from a Rigid Heavy Vehicle When Including Road Crossfall

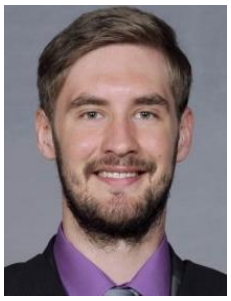

AJ STEENKAMP
A Mechanical Engineer at the CSIR who has an MSc in heavy vehicle dynamics from Wits University. He is an accredited PBS and road infrastructure assessor with an interest in the effect of heavy vehicles on dynamic road damage.

F KIENHÖFER
A research consultant conducting PBS assessments and visiting associate professor at Wits University researching brakes, heavy vehicle safety, high productivity vehicles, and sustainable road freight transport.

CC DE SAXE
Senior Research Associate at the Centre for Sustainable Road Freight at Cambridge University, and Visiting Lecturer at the University of the Witwatersrand. Holds a PhD in engineering from Cambridge University.

Abstract

Previous research investigating the dynamic road wear produced by heavy vehicles has not included the effect of road crossfall. This study shows that road crossfall, even at values as low as 1%, has a significant effect on the predicted dynamic road wear. A model of a rigid vehicle that includes rolling and pitching motion was developed for the analysis. The normalized 95th percentile aggregate fourth-power force is used as the road damage criteria. For the vehicle studied, a 24% increase in road damage is predicted for a crossfall value of 2% as compared to not modelling the crossfall, at a typical highway speed of 80 km/h and road roughness of 2 m/km. Road crossfall therefore plays a significant role in the dynamic road damage produced by heavy vehicles.

Keywords: Heavy vehicles, dynamic road wear, crossfall, rigid vehicle

1. Introduction

Transport logistics are one of the key aspects of any economy and, according to the latest Logistics Barometer, constitute 11.8% of South Africa's GDP. In South Africa, approximately 85% of freight is transported by road (Havenga, et al., 2016). The value of the paved road network in South Africa is estimated to be approximately $145 billion and represents one of the country's most important assets. South Africa has a road maintenance backlog of $4.2 billion, which has led to a national network where currently 78% of the roads are older than their intended design life (Krygsman & Van Rensburg, 2017). It is therefore crucial to minimize the road wear caused by heavy vehicles which, if overloaded, can account for more than 60% of all road damage caused (Krygsman & Van Rensburg, 2017). Minimizing pavement damage requires a detailed understanding of the physics and mechanisms that cause this damage.

A heavy vehicle's suspension is critical to the road-friendliness of the vehicle. A study by the Organisation for Economic Cooperation and Development (OECD) found that a dynamic

analysis of a well-damped suspension system will generally predict between 5% and 10% more road damage than the statically-loaded case analysis (Hjort, et al., 2008). In contrast, a poorly damped suspension will cause between 20% and 40% more road damage when dynamic effects are considered (Hjort, et al., 2008). A substantial proportion of models developed to calculate dynamic tyre forces and pavement damage are limited to quarter-car models. Such models are useful, but information regarding the vehicle roll and pitching are not captured.

As a result, most dynamic road wear studies do not consider the effects of road crossfall. In this paper, we show that incorporating the effect of road crossfall in a dynamic analysis leads to a substantial difference in the predicted left and right road damage produced by heavy vehicles.

2. Background

The quarter-car model has been the most widely adopted model for simulating dynamic tyre forces. The quarter-car model is not however able to capture complex suspension nonlinearities and the complexities of heavy vehicle body motion, though the frequency content of the quarter-car model is sufficiently accurate (Buhari, et al., 2013). This has been verified by Hardy and Cebon (Hardy & Cebon, 1994). In general, researchers keep models realistic but simple to minimize complexity and reduce computation time (Buhari, et al., 2013).

When higher degree-of-freedom models are developed, researchers often ignore body roll motion or conclude that its influence is negligible. As such, dynamic road wear models are usually limited to either quarter-car or half-car models that utilize pitch-plane motion (Cebon, 1999). Cebon specifically states that: “A two-dimensional model (pitch-plane) should be satisfactory for predicting the tyre forces of typical leaf-spring articulated vehicles with well damped suspension modes, operating under typical conditions of speed and road roughness”. He however adds that: “It may therefore be necessary to use a three-dimensional model when the unsprung mass roll modes contribute significantly to dynamic tyre forces”. This would be the case if the crossfall of a road profile is included in the model.

The equivalent single axle load (ESAL) or load equivalency factor (LEF) is commonly used to quantify road damage due to the static loads. The ESAL damage is calculated as shown in Equation 1 (van der Walt, et al., 2018).

$$ESAL = LEF = \left(\frac{Actual\ axle\ load}{Reference\ load}\right)^n \tag{1}$$

Where *n* is an appropriate exponent to quantify the damage on a specific pavement. This value is usually taken as 4 but values greater than 7 have been proposed (van der Walt, et al., 2018).

To quantify dynamic road damage, the normalized 95th percentile aggregate fourth-power tyre force can be used. The aggregate tyre force is calculated using Equation 2 (Cebon, 1988; Cebon, 1999).

$$A_k^n = \sum_{j=1}^{N_a} P_{jk}^n \quad k = 1,2,3, \dots, Ns \tag{2}$$

Where A_k^n is the aggregate n^{th} power force, P_{jk} is the force applied by tyre j to location or station k on the road, N_a is the number of axles on the vehicle and N_s is the number of points or stations of interest along the road. The power (n) is chosen based on the type of road damage that is

being considered. For flexible pavements, a value of $n = 1$ is best suited for permanent road deformation and $n = 4$ is best suited for fatigue damage (Cebon, 1988; Cebon, 1999). It has been found that the ratio of the instantaneous fourth power force to the static fourth power force can exceed 3 which indicates how the peak dynamic loads can be substantially higher at certain locations and cause more damage at specific sections (Cebon, 1988; Cebon, 1999).

The ratio of the 95th percentile aggregate force to the static aggregate force is often used as the road damage criteria in numerous road studies. It is also referred to as the dynamic aggregate force coefficient (DAFC) and can be estimated from Equation 3 (Cebon, 1988; Cebon, 1999).

$$DAFC = \frac{1.65 \cdot \sigma_A^4}{m_{A^4}} + 1 \quad (3)$$

Where σ_{A^4} is the standard deviation of the fourth power aggregate forces and m_{A^4} is the static fourth power force (Cebon, 1988; Cebon, 1999).

Ihs and Magnusson (2000) state that the effect of road crossfall is negligible. Other previous research projects and guidelines focus primarily on the effect of road roughness, vehicle speeds, loading of the heavy vehicles and suspension characteristics. When crossfall is referred to, emphasis is placed on its vital importance in preserving road infrastructure by ensuring adequate drainage (Bowen, 2017).

In contrast to Ihs and Magnusson, van der Walt et al. noticed that the left wheel path (LWP) always had more rutting than the right wheel path (RWP) (van der Walt, et al., 2018). The study in New Zealand (vehicles drive on the left side of the road) by Ihs and Magnusson found the ESAL value can double when using actual wheel loads with different left and right values due to the crossfall as compared with using equal left and right wheel loads. This study also included the effect of the axle width, height of the centre of mass, the percentage crossfall and the rutting depth. The study concluded that there are no other mechanisms that can account for the difference in rutting between left and right tracks except for the road crossfall (van der Walt, et al., 2018). The study however did not include any dynamic loading which provides little information of the performance over different operating conditions as is the aim of this study.

A South African study (2019) also concluded that crossfall has a considerable effect on dynamic road damage. This study used TruckSim® to investigate the dynamic road wear of a Performance-Based Standards heavy vehicle at different crossfall values and used the South African Mechanistic Empirical Design Method for calculating the road wear produced (Steenkamp, et al., 2019)

The latest study on this topic of road wear produced by road crossfall was conducted in 2020. The study showed that road crossfall has a definite impact on the difference in left and right wheel path loads (Kakara & Chowdary, 2020). The results showed that the load differences increase approximately linearly with crossfall or camber.

The study further investigated the impact of different road roughness values and crossfall on the pavement strains. The study shows that ignoring crossfall leads to an underestimation of the tyre loads and road damage (Kakara & Chowdary, 2020). The study however used a multibody simulation software package and not a model developed from first principles as is used in this study. The vehicle selected also had a very low centre of gravity which would underestimate the damage produced when including road crossfall.

No work could be found that implements a model developed from first principles to predict the dynamic forces of heavy vehicles when including road crossfall. This study addresses this research gap and illustrates that a simple pitch-roll heavy vehicle model is sufficiently accurate to capture this phenomenon.

3. Methodology

A full-car heavy vehicle model that includes pitch and rolling motion was developed using Simulink® in Matlab®. The dual track road profiles were similarly created using Matlab®. The ISO 8608 method was used to create the first road profile and the assumption of surface homogeneity and isotropy was used to generate the second correlated road profile. The IRI values considered in this study vary from 0.5 m/km to 10 m/km. This represents a range from superhighways to poorly managed paved roads (COTO Road Network Management Systems Committee, 2007). Road crossfall values between 0% to 5% are included in the road profiles as this corresponds to typical values found in South Africa and across the world. Vehicle speeds between 40 km/h and 120 km/h were simulated. This represents minimum and maximum speeds in South Africa. Heavy vehicles are technically limited to 80 km/h but from telematics data it has been observed that in practice some heavy vehicles travel at speeds greater than 120 km/h. The road profiles used in the simulation were 1 km long.

The validation of the full car model was done using TruckSim 2019.1®. The software is a commercially available multibody simulation tool capable of assessing the performance of complex vehicle models performing complex manoeuvres. A model developed from first principles has the advantage of requiring significantly cheaper software to develop and has quicker run times compared to a commercially available software package (TruckSim 2019.1®).

A single 4x2 full-car heavy vehicle model was developed that includes the vehicle parameters that most influence the rolling motion of a heavy vehicle. The representative vehicle parameters were obtained from various sources based on other heavy vehicle studies and have been summarized in Table 3-1. Linear models were used for suspension components to simplify the analysis. It should be noted that a rear suspension stiffness was selected to represent a value between air and steel suspension to obtain an "average" result between the two suspension types.

Table 3-1: Heavy vehicle parameters used

Parameter	Symbol	Unit	Value
Sprung mass	m_s	kg	12 500
Unsprung mass front	m_{uf}	kg	706
Unsprung mass rear	m_{ur}	kg	1 000
Track width front	$2 \cdot T_f$	m	2
Track width rear	$2 \cdot T_r$	m	2
Spring track width front	$2 \cdot S_f$	m	1.2
Spring track width rear	$2 \cdot S_r$	m	1.2
Tyre vertical spring stiffness front	k_{tf}	N/m	1 000 000
Tyre vertical spring stiffness rear	k_{tr}	N/m	1 000 000
Spring stiffness front	k_f	N/m	200 000
Spring stiffness rear	k_r	N/m	400 000

Distance front to CoG	$\boldsymbol{a}$	m	1.95
Distance rear to CoG	$\boldsymbol{b}$	m	1.55
Front RC height	$\boldsymbol{h_{1f}}$	m	0.6
Rear RC height	$\boldsymbol{h_{1r}}$	m	0.6
Front unsprung mass height	$\boldsymbol{h_{2f}}$	m	0.5
Rear unsprung mass height	$\boldsymbol{h_{2r}}$	m	0.5
Sprung mass height	$\boldsymbol{h}$	m	2
Damper value front	$\boldsymbol{c_f}$	Ns/m	5 000
Damper value rear	$\boldsymbol{c_r}$	Ns/m	10 000
Roll inertia sprung mass	$\boldsymbol{I_{sr}}$	kg·m^2	24 201
Pitch inertia	$\boldsymbol{I_{sp}}$	kg·m^2	34 917
Unpsrung mass roll inertia front	$\boldsymbol{I_{uf}}$	kg·m^2	572
Unpsrung mass roll inertia rear	$\boldsymbol{I_{ur}}$	kg·m^2	810
Front tyre relaxation length	$\boldsymbol{L_f}$	m	1.0
Rear tyre relaxation length	$\boldsymbol{L_r}$	m	1.0

The dynamic road damage criterion considered is the normalized fourth power aggregate force.

4. Model Development and Validation

The two main aspects developed in this paper are the dual track road profiles and the heavy vehicle model which are discussed in separate subsections.

4.1 Dual track road profile validation

The dual track road profiles were created and validated using the ISO 8608 method and the assumption of isotropy. To ensure that the road profiles have been created correctly, the smoothed power spectral density (PSD) and cross PSD, IRI and coherence value of each road profile was calculated and found to be within acceptable limits of the design specifications. Detailed results have been excluded due to space limitations in this paper.

4.2 Heavy vehicle model development and validation

No work could be found that implements a model from first principles to determine the dynamic forces of heavy vehicles when including road crossfall of a road profile. For this study, a 9 degree of freedom (DoF) model was developed.

The pitching motion of the sprung mass (see Figure 4.1) on a flat surface is described by Equation 4.

$$\begin{aligned}&(I_{sp} + m_s \cdot (h - h_1)^2) \cdot \ddot{\Phi}_{sy} = (F_{srl}+F_{drl} + F_{srr}+F_{drr}) \cdot b \\ &-(F_{sfl}+F_{dfl} + F_{sfr}+F_{dfr}) \cdot a\end{aligned} \tag{4}$$

Where I_{sp} is the sprung mass pitching moment of inertia, m_s is the sprung mass, h is the height of the sprung mass from the floor, h_1 is the roll centre height from the floor, $\ddot{\Phi}_{sy}$ is the sprung mass pitch angular acceleration, a is the distance from the front axle to the sprung mass center of gravity, b is the distance from the rear axle to the sprung mass centre of gravity. The first

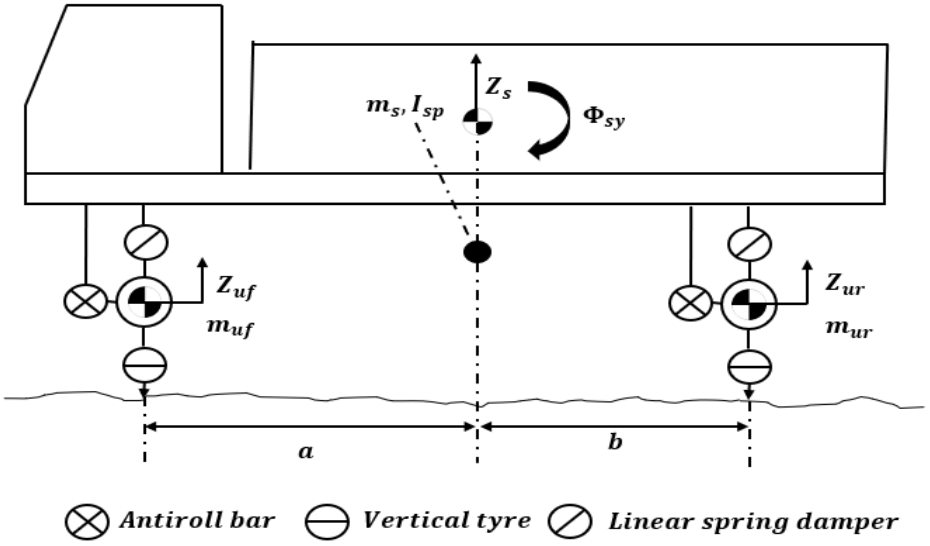

Figure 4-1: Pitching motion of the developed heavy vehicle model

letter of the force subscript refers to whether it is a spring or damper force (F_s refers to a spring force and F_d refers to a damper force), while the last two letters refer to the position with the second letter referring to either front or rear and the last letter referring to left or right. As an example, F_{drl} refers to the damper force of the rear left tyre position.

The rolling motion of the sprung mass (see Figure 4.2) is described by Equation 5.

$$\begin{aligned}(I_{sr} + m_s(h-h_1)^2)\cdot\ddot{\theta}_{sx} &= m_s\,(h-h_1)\cdot\left(\ddot{Y}_s + g\cdot(\theta_{sx}+E_s)\right)\\ &+\left(F_{sfl}+F_{dfl}-F_{sfr}-F_{dfr}\right)\cdot S_f + (F_{drl}+F_{drl}-F_{srr}-F_{drr})\cdot S_r\\ &-R_f\cdot(\theta_{sx}-\theta_{ufx}) - R_r\cdot(\theta_{sx}-\theta_{urx})\end{aligned} \tag{5}$$

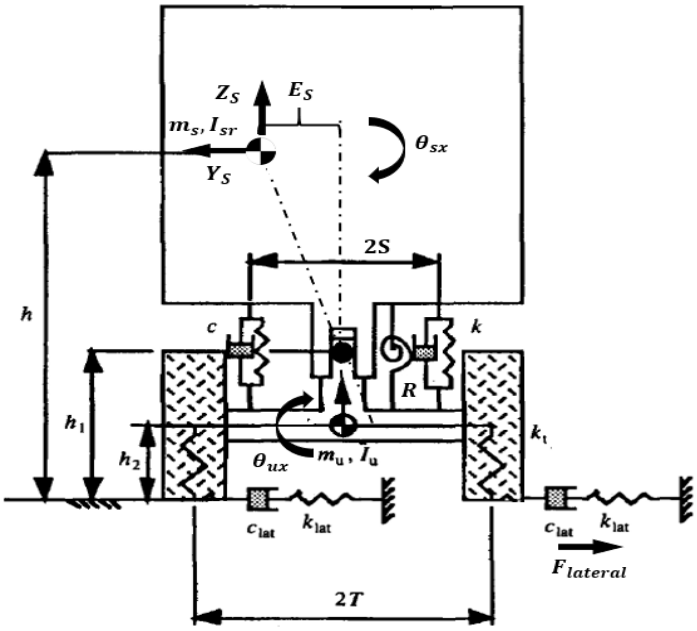

Figure 4-2: Rolling motion of heavy vehicle model modified from (Cole & Cebon, 1996)

Where I_{sr} is the sprung mass rolling motion moment of inertia, $\ddot{\theta}_{sx}$ is the sprung mass rolling angular acceleration, $\ddot{Y}$ is the sprung mass lateral acceleration, g is the gravitational acceleration, θ_{sx} is the sprung mass roll angle, E_s is the lateral eccentricity of the sprung mass. S_f is half of the front spring track, S_r is half of the rear spring track, R_f is the front anti-roll bar stiffness, R_r is the rear anti-roll bar stiffness, θ_{sx} is the sprung mass roll angle, θ_{ufx} is the front unsprung mass roll angle, θ_{urx} is the rear unsprung mass roll angle. Other symbols have been previously introduced and are available in the list of symbols.

The vertical motion of the sprung mass is described by Equation 6.

$$m_s \cdot \ddot{Z}_s = F_{sfl} + F_{dfl} + F_{sfr} + F_{dfr} + F_{srl} + F_{drl} + F_{srr} + F_{drr} \quad (6)$$

Where $\ddot{Z}_s$ is the vertical acceleration of the sprung mass.

The lateral motion of the sprung mass on a flat surface is described by Equation 7.

$$m_s \cdot \ddot{Y}_s = F_{Lfa} + F_{Lra} \quad (7)$$

Where $\ddot{Y}_s$ is the lateral acceleration of the sprung mass, F_{Lfa} is the lateral force on the front axle and F_{Lra} is the lateral force on the rear axle. It should be noted this is only the dynamic forces and does not include a constant lateral force produced by the road crossfall.

The vertical motion of the front and rear unsprung masses is described by Equation 8 and Equation 9.

$$m_{uf} \cdot \ddot{Z}_{uf} = F_{sfl} + F_{dfl} + F_{sfr} + F_{dfr} + F_{tfl} + F_{tfr} \quad (8)$$

$$m_{ur} \cdot \ddot{Z}_{ur} = F_{srl} + F_{drl} + F_{srr} + F_{drr} + F_{trl} + F_{trr} \quad (9)$$

Where m_{uf} and m_{ur} are the front and rear unsprung masses, $\ddot{Z}_{uf}$ and $\ddot{Z}_{ur}$ are the front and rear unsprung vertical accelerations.

The lateral force generating properties of a tyre can be described by using a first order equation of a spring and damper in series with time constant τ_{lat} (Loeb, 1990). The damping value is obtained using Equation 10.

$$c_{lat} = \frac{C_c \cdot F_{tyre\ vertical}}{V} \quad (10)$$

Where c_{lat} is the lateral tyre damping value, C_c is the lateral tyre cornering coefficient, $F_{tyre\ vertical}$ is the vertical tyre force and V is the longitudinal velocity of the vehicle.
The stiffness of the spring (k_{lat}) is obtained using Equation 11 (Cole & Cebon, 1996).

$$k_{lat} = \frac{C_c \cdot F_{tyre\ vertical}}{\tau_{lat} \cdot V} \quad (11)$$

The term $\tau_{lat} \cdot V$ is referred to as the relaxation length L of the tyre (Cole & Cebon, 1996). There are large variations in the reported relaxation length of tyres. Cebon and Cole quote this value to be equal to the tyre contact patch length which is approximately 0.3 m (Cole & Cebon, 1996). Other sources quote this value as between 25% and 50% of the tyre circumference (Vehicle Dynamics Group, Division Vehicle and Autonomous Systems, 2017). A reasonable estimate of the relaxation length is twice the tyre radius (Vantsevich & Gray, 2015) and is often recommended in TruckSim® (Mechanical Simulation, 2019). This value of twice the tyre radius equates to 32% of the tyre circumference which falls in the range of 25% to 50% of the tyre circumference. For this study, the relaxation length is assumed to be 1 m which is twice the tyre loaded radius.

The front and rear lateral friction force produced by the road crossfall (see Figure 4.3) is calculated as shown in Equation 12 and Equation 13 This result is obtained through a simple moment balance.

$$F_{latcf} = m \cdot g \cdot \frac{b}{Wb} \cdot sin(\Psi) \tag{12}$$

$$F_{latcr} = m \cdot g \cdot \frac{a}{Wb} \cdot sin(\Psi) \tag{13}$$

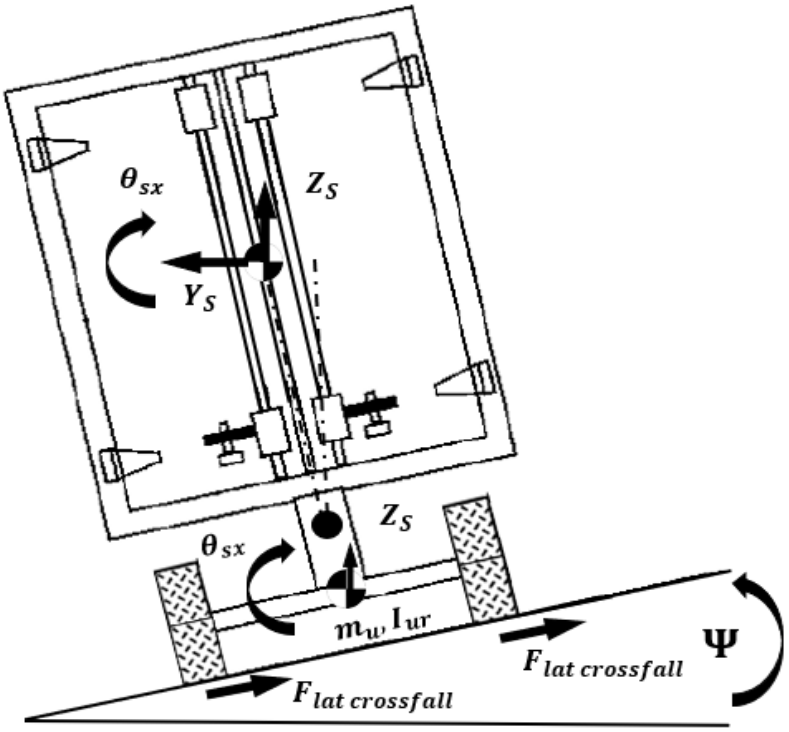

Figure 4-3: Rolling motion of heavy vehicle when including crossfall modified from (Cole & Cebon, 1996)

The equations of motion for the unsprung masses as shown in Equation 14 and Equation 15.

$$(I_{uf} + m_{uf} \cdot (h_1 - h_2)^2) \cdot \ddot{\theta}_{ufx} = m_{uf}\,(h_1 - h_2) \cdot \left(g \cdot \theta_{ufx}\right)$$
$$+\left(F_{sfl} + F_{dfl} - F_{sfr} - F_{dfr}\right) \cdot S_f + R_f \cdot \left(\theta_{sx} - \theta_{ufx}\right) + \left(F_{tfl} - F_{tfr}\right) \cdot T_f + F_{latcf} \tag{14}$$

$$(I_{ur} + m_{ur} \cdot (h_1 - h_2)^2) \cdot \ddot{\theta}_{urx} = m_{ur}\,(h_1 - h_2) \cdot (g \cdot \theta_{urx}) \\ +(F_{srl} + F_{drl} - F_{srr} - F_{drr}) \cdot S_r + R_r \cdot (\theta_{sx} - \theta_{urx}) + +(F_{trl} - F_{trr}) \cdot T_r + F_{latcr} \qquad (15)$$

The heavy vehicle model was validated under several operating conditions. It was found that the average absolute error between TruckSim® and the model of the fourth power aggregate forces calculated over each point is less than 3% for typical highway operating conditions (road roughness values around 2 m/km and vehicle speed of 80 km/h). The maximum recorded error was 15% for an extreme operating condition of 5% crossfall, 120 km/h and 10 m/km IRI. The percentage error between TruckSim® and the model for the 95th percentile aggregate fourth-power force was less than 2% for typical operating conditions and a maximum value of 6% was recorded. An example of the comparison of the fourth power aggregate forces from the model and TruckSim® is shown in Figure 4-4.

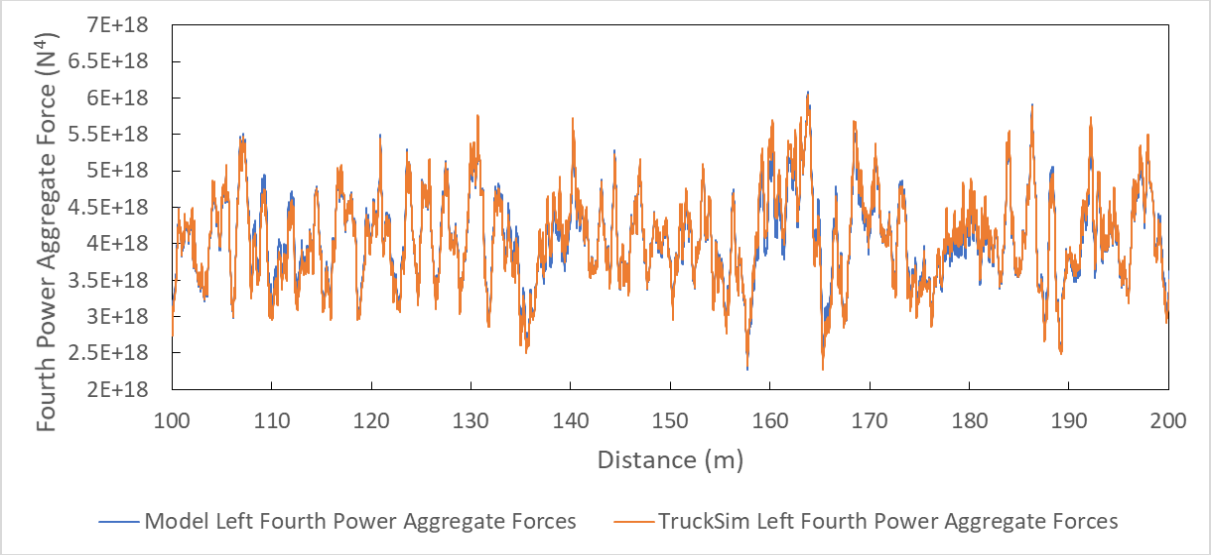

Figure 4-4: Comparison of the left fourth power aggregate foces for a road roughness of 2 m/km, vehicle speed of 80 km/h and 2% crossfall

5. Results

The fourth power aggregate forces are normalized by 3.2x10^{18} N^4, representing the fourth power aggregate force of the static vehicle. The normalized 95th percentile aggregate fourth power force for the left side of the vehicle is shown for all operating conditions in Figure 5-1. The percentage difference in the left and right 95th percentile aggregate fourth-power forces is shown in Table 5-1. It should be noted that in South Africa the vehicles travel on the left side and therefore forces increase on the left side as crossfall increases.

Figure 5-1 shows that the road crossfall is approximately linearly related to the fourth power aggregate forces and increases on the left side and decreases on the right side as the crossfall increases. For a typical highway roughness value of 2 m/km and vehicle speed of 80 km/h, the left side normalized damage ranges from 1.293 at a road crossfall of zero to 2.189 at a road crossfall of 5%. This shows that a small change of 5% in the crossfall, increased the normalized damage by almost 70%. At a more typical crossfall value of 2% the normalized damage coefficient on the left side is 1.608. This is an increase of 24%. The dynamic damage is more than the static damage. Simply using the static fourth power force method severely underestimates the predicted road damage. At a 0% crossfall it would have led to an underestimation of 29.3% at typical highway operating conditions.

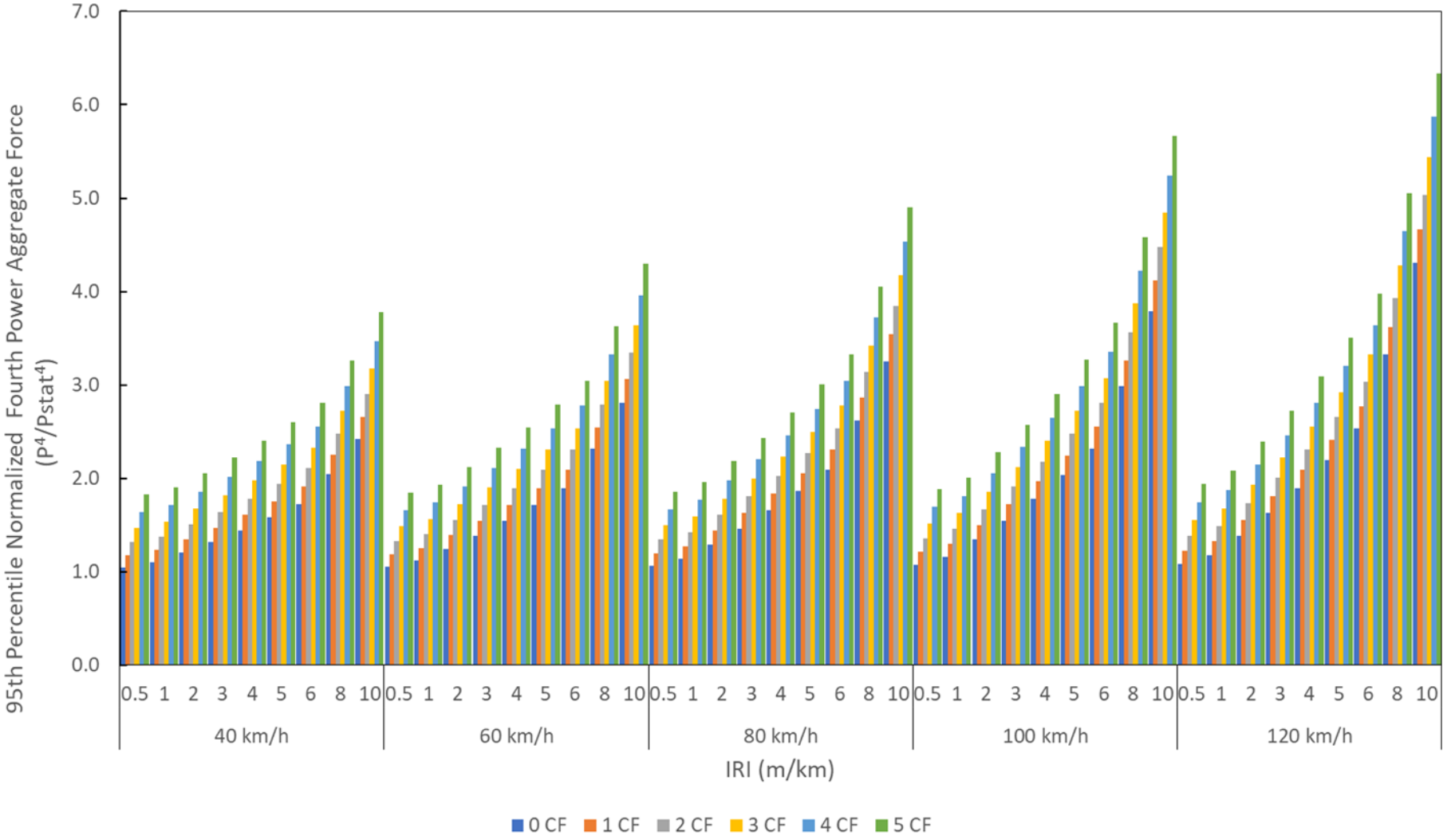

Figure 5-1: Left normalized 95th percentile fourth power aggregate force of the vehicle model over all operating conditions

Table 5-1: The percentage difference in the left and right 95th percentile aggregate fourth-power force

	IRI (m/km) →	0.5	1	2	3	4	5	6	8	10
	Crossfall (%)	Percentage Difference Between Left and Right (%)								
40 km/h	0	-0.01	-0.02	-0.05	-0.06	-0.10	-0.14	-0.20	-0.32	-0.36
	1	23.52	23.22	22.63	22.02	21.43	20.91	20.41	19.29	18.28
	2	46.46	45.89	44.77	43.68	42.61	41.61	40.59	38.62	36.72
	3	68.25	67.48	65.92	64.39	62.88	61.43	60.06	57.18	54.64
	4	88.45	87.52	85.61	83.70	81.90	80.10	78.33	74.91	71.67
	5	106.73	105.69	103.55	101.43	99.35	97.32	95.29	91.45	87.75
60 km/h	0	-0.03	-0.05	-0.09	-0.13	-0.14	-0.12	-0.06	0.00	-0.02
	1	23.48	23.14	22.47	21.81	21.18	20.71	20.14	19.23	18.28
	2	46.42	45.74	44.51	43.32	42.15	41.04	40.04	38.16	36.30
	3	68.17	67.27	65.51	63.88	62.26	60.71	59.21	56.39	53.85
	4	88.34	87.27	85.10	83.03	81.08	79.16	77.31	73.81	70.52
	5	106.61	105.43	103.02	100.66	98.44	96.26	94.07	90.04	86.15
80 km/h	0	-0.10	-0.18	-0.30	-0.48	-0.69	-0.82	-0.92	-1.15	-1.75
	1	23.33	22.85	21.94	21.05	20.26	19.47	18.65	17.25	15.74
	2	46.21	45.35	43.73	42.24	40.73	39.33	37.93	35.50	33.03
	3	67.94	66.79	64.55	62.47	60.45	58.51	56.69	53.21	49.87
	4	88.10	86.74	84.01	81.47	79.03	76.66	74.40	70.06	65.95
	5	106.37	104.87	101.87	98.97	96.22	93.58	90.90	86.01	81.21
100 km/h	0	0.13	0.25	0.48	0.64	0.76	0.95	1.05	1.16	0.98
	1	23.56	23.29	22.69	22.05	21.44	20.92	20.41	19.20	18.15
	2	46.37	45.67	44.34	43.00	41.72	40.53	39.34	37.02	34.95
	3	67.98	66.99	65.02	63.07	61.20	59.46	57.61	54.22	51.10
	4	87.95	86.81	84.27	81.90	79.60	77.27	75.00	70.71	66.78
	5	106.00	104.78	101.89	99.14	96.49	93.87	91.27	86.31	81.54
120 km/h	0	0.09	0.18	0.36	0.56	0.75	0.84	0.96	1.25	1.17
	1	23.62	23.06	22.25	21.54	20.89	20.17	19.57	18.49	17.32
	2	46.51	45.65	43.74	42.22	40.74	39.26	37.92	35.50	33.29
	3	68.00	67.08	64.31	62.02	59.96	57.90	55.94	52.29	48.90
	4	87.77	86.78	83.84	80.57	77.95	75.51	73.06	68.37	64.10
	5	105.79	104.64	101.63	97.97	94.62	91.73	89.07	83.70	78.39

Considering the right side normalized fourth power forces at a vehicle speed of 80 km/h and road roughness of 2 m/km, the values change from 1.297 at a crossfall of 0% to 0.711 at a road crossfall of 5%. This is a decrease of 46% which is much less than the increase of 70% on the left side of the vehicle. At a more typical crossfall value of 2% the normalized damage is 1.031 which shows a decrease of 21%. This is a value closer to the increase of 24% on the right side. Therefore, the rate of increase in damage is higher on the left side compared to the rate of decrease in damage on the right side. These differences are exacerbated at higher road roughness values and vehicle speeds. For example, using a road roughness of 4 m/km and a road crossfall of 3% which is typical on more urban roads, the normalized road damage is 2.238 on the left side and 1.199 on the right side. This shows that the road damage on the left is more than double the static value and, on the right, almost 20% greater than the static value.

6. Conclusions and Recommendations for Future Work

This study shows that the road crossfall has a significant effect on the road wear produced by heavy vehicles, even for values as low as 1%. This report supports other recent studies that have found a difference in the road roughness values and rutting values of the left and right wheel paths.

Future work can expand on these findings by studying the effect of different heavy vehicle parameters on the dynamic road damage of a heavy vehicle when including road crossfall. Models can also be expanded to include non-linear suspension and damping values. Additional vehicle units can also be added to study the effect of road crossfall on different vehicle combinations. Other coherence functions for road profiles can also be investigated.

7. References

- Bowen, C., 2017. *The importance of road drainage.* [Online] Available at: https://www.newenglandsealcoating.com/the-importance-of-road-drainage/ [Accessed 28 September 2020].
- Buhari, R., Rohani, M. M. & Abdullah, M. E., 2013. Dynamic load coefficient of tyre forces from truck axles. *Applied Mechanics and Materials,* Volume 405-408, pp. 1900-1911.
- Cebon, D., 1988. *Road damaging effects of dynamic axle loads.* Canada, s.n.
- Cebon, D., 1999. *Handbook of vehicle-road interaction.* Lisse, Netherlands: Swets & Zeitlinger.
- Cole, D. J. & Cebon, D., 1996. Truck suspension design to minimize road damage. *Journal of Automobile Engineering,* Volume 210.
- COTO Road Network Management Systems Committee, 2007. *Guidelines for network level measurement of road roughness,* s.l.: s.n.
- Hardy, M. & Cebon, D., 1994. Importance of speed and frequency in flexible pavement. *Journal of Engineering Mechanics,* 120(3), pp. 463-482.
- Havenga, J. H., Simpson, Z. P., de Bod, D. & Braun, M., 2016. *A Logistic Barometer for South Africa: Towards sustainable freight mobility,* s.l.: Stellenbosch University.
- Hjort, M., Haraldsson, M. & Jansen, J. M., 2008. *Road wear from heavy vehicles- an overview,* Borlange, Sweden: NVF committee Vehicles and Transports.
- Ihs, A. & Magnusson, G., 2000. *The significance of various road surface properties fo traffic and surroundings.,* s.l.: Swedish National Road and Transport Research Intstitute.
- Kakara, S. & Chowdary, V., 2020. Effect of pavement roughness and transverse slope on the magnitude of wheel loads. *Arabian Journal for Science and Engineering,* Volume 45, pp. 4405-4418.
- Krygsman, S. & Van Rensburg, J., 2017. *Funding for Roads in South Africa: Understanding the principles of fair and efficient road user charges,* Stellebosch: ResearchGate.
- Loeb, J. S., 1990. Lateral stiffness, cornering stiffness and relaxation length of the pneumatic tyre. *SAE Proc.*
- Mechanical Simulation, 2019. *Tire Models,* s.l.: Mechanical Simulation.
- Steenkamp, A. J., Berman, R., Kemp, L. & De Saxe, C. C., 2019. *The effect of road crossfall on road wear caused by heavy vehicles.* s.l., s.n.
- van der Walt, J. D., Scheepbouwer, E. & Tighe, S. L., 2018. Differtial rutting in Canterbury New Zealand, and its relation to road camber. *international Journal of Pavement Engineering,* 19(9), pp. 798-804.
- Vantsevich, V. & Gray, J. P., 2015. *Relaxation length review and time constant analysis for agile tire dynamics control.* Massachusetts, s.n.
- Vehicle Dynamics Group, Division Vehicle and Autonomous Systems, 2017. *Vehicle Dynamics: Compendium,* s.l.: Chalmers.